# Equilibrium and kinetics study on removal of arsenate ions from aqueous solution by CTAB/$TiO_2$ and starch/CTAB/$TiO_2$ nanoparticles: a comparative study

Pankaj Gogoi, Debasish Dutta and Tarun Kr. Maji

## ABSTRACT

We present a comparative study on the efficacy of $TiO_2$ nanoparticles for arsenate ion removal after modification with CTAB (N-cetyl-N,N,N-trimethyl ammonium bromide) followed by coating with starch biopolymer. The prepared nanoparticles were characterized by Fourier transform infrared spectroscopy (FT-IR), X-ray diffractometry (XRD), thermogravimetry, scanning electron microscopy (SEM) and electron dispersive X-ray analysis (EDX). The removal efficiency was studied as a function of contact time, material dose and initial As(V) concentration. CTAB-modified $TiO_2$ showed the highest arsenate ion removal rate (~99% from 400 μg/L). Starch-coated CTAB-modified $TiO_2$ was found to be best for regeneration. For a targeted solution of 400 μg/L, a material dose of 2 g/L was found to be sufficient to reduce the As(V) concentration below 10 μg/L. Equilibrium was established within 90 minutes of treatment. The sorption pattern followed a Langmuir monolayer pattern, and the maximum sorption capacity was found to be 1.024 mg/g and 1.423 mg/g after starch coating and after CTAB modification, respectively. The sorption mechanisms were governed by pseudo second order kinetics.

**Key words** | CTAB modification, kinetics, regeneration, sorption capacity, starch coating

**Pankaj Gogoi**
**Debasish Dutta**
**Tarun Kr. Maji** (corresponding author)
Department of Chemical Sciences,
Tezpur University,
Assam 784028,
India
E-mail: *tkm@tezu.ernet.in*

## ABBREVIATIONS

| | |
|---|---|
| ATC | arsenic-treated SPC |
| CMT | CTAB-modified $TiO_2$ |
| CTAB | N-cetyl-N,N,N-trimethyl ammonium bromide |
| SPC | starch-coated CMT |
| UTi | unmodified $TiO_2$ |

## INTRODUCTION

$TiO_2$ is currently considered as the most versatile nanomaterial. It has a wide range of applications in different fields (Xiaobo & Samuel 2007). These are attributed to its low cost, low toxicity, photostability in solution, redox selectivity and strong oxidizing power of holes. The application of $TiO_2$ at the nanoscale further improves efficiency due to the high surface area, large pore volume and presence of high affinity surface hydroxyl groups (Daimei *et al.* 2006; Gupta *et al.* 2012). $TiO_2$ and its different modified forms have also drawn the attention of researchers in the field of the removal of contaminants from water. It is capable of removing heavy metals as well as arsenite and arsenate from contaminated water (Gautham *et al.* 2010).

Gupta & Tripathi (2011) reviewed the use of $TiO_2$ for environmental clean-up of organic pollutants through photo-oxidation. Xu *et al.* (2007) studied the photocatalytic degradation of organic arsenic to inorganic form by $TiO_2$ and successful sorption on its surface.

Debnath & Ghosh (2009) applied nanostructured hydrous titanium oxide to adsorb Ni(II) from natural and

doi: 10.2166/wh.2016.127

industrial wastewater. The sorption of Se(IV) on $TiO_2$ (anatase) was investigated by Keliang *et al.* (2009). Ghosh *et al.* (2003) and Barakat (2005) studied the use hydrous titanium oxide for adsorption of Cr(VI) and Cu(II), respectively.

Xu *et al.* (2010) prepared hydrous titanium dioxide ($TiO_2.xH_2O$) by one-step hydrolysis. The adsorption capacity of sorption of As(III) was found to be very high and was pH dependent. The sorption of As(III) and As(V) on commercially available $TiO_2$ was also found to be dependent on pH as well as initial ion concentration (Dutta *et al.* 2004). Bang *et al.* (2005) experimented with a novel granular $TiO_2$ for removal of groundwater arsenic and found that more arsenate was adsorbed than arsenite on $TiO_2$ at pH 7.0. Nakajima *et al.* (2005) investigated the use of $TiO_2$ photocatalyst and adsorbent for removal of As(V) under photo-irradiation.

Barakat (2005) studied photocatalytic degradation using UV-irradiated $TiO_2$ suspension for destroying complex cyanide with a simultaneous removal of copper. Kajitvichyanukul *et al.* (2005) prepared $TiO_2$ thin films immobilized on glass plates for removal of Cr(VI).

Heterogeneous photocatalytic oxidation of arsenite to arsenate in aqueous $TiO_2$ suspensions has also been proved recently to be an effective and environmentally acceptable technique for the remediation of arsenite-contaminated water. Zhang & Itoh (2006) performed a process using an adsorbent developed by loading iron oxide and $TiO_2$ on municipal solid waste melted slag for oxidation of arsenite to arsenate.

However, the dispersibility, reusability and leaching of particles are a major concern for the use of $TiO_2$ in water purification. The nanoparticles have very high surface energy. Therefore, they tend to agglomerate so that they can reduce their surface energy by decreasing the surface area and thus stabilize (Gupta *et al.* 2012). Certain modifications are necessary to overcome these limitations. Adequate surface functionalization and coating with polymeric materials, for example, are some of the promising aspects regarding selectivity and aqueous stability of this material.

Use of surfactant-like CTAB increases the stability of $TiO_2$ nanoparticles in water by forming micelles around them and thus can enhance the dispersibility of the particles in aqueous medium (Deka & Maji 2011). CTAB also contains a hydrophilic end (Miao *et al.* 2014), which might enhance the solubility of modified $TiO_2$ particles in aqueous medium. Thus some particles may get leached in to water during wastewater treatment. This difficulty may be avoided by the use of supporting materials or by coating the nanoparticles with polymeric materials.

Starch, one of the cheapest and nontoxic polymers, is abundantly available in nature. Starch and starched-based materials used as bio-compatible materials have been cited in the literature (Marques *et al.* 2002; Saikia *et al.* 2010). He & Zhao (2005) have reported the advantage of coating starch onto bimetallic nanoparticles (Fe-Pd) for degradation of chlorinated hydrocarbons in water. A significant improvement in arsenic removal rate from brine by using starch-coated magnetite nanoparticles has been reported (An *et al.* 2011). Stabilization with starch causes less agglomeration and improves removal rate compared to the bare nanoparticles. The processing of starch for stabilizing nanomaterials is quite easy. Starch can be easily solubilized in hot water and re-precipitated by simply adding acetone or ethanol. The coating of the nanomaterial by starch can be done in aqueous medium without using any other toxic chemicals.

The aim of the present work is to prepare CTAB-modified $TiO_2$ nanoparticles and stabilize them by coating with starch, and finally use the particles in the treatment of As (V)-contaminated water. A comparative study was made using unmodified $TiO_2$ (UTi), CTAB-modified $TiO_2$ (CMT) and starch-coated CMT (SPC). Low concentrations of arsenic solutions were used in the experiments considering the practical applicability of the material.

## MATERIALS AND METHODS

Analytical grade nanosized $TiO_2$ (mixture of rutile and anatase), potassium sulfate ($K_2SO_4$), and sodium arsenate dibasic heptahydrate ($HAsNa_2O_4.7H_2O$) were purchased from Sigma-Aldrich. Starch polymer was purchased from SRL, India. Gluteraldehyde solution (25%), used as cross-linking agent, and di-sodium hydrogen phophate ($Na_2HPO_4$) were purchased from E-Merck, India. CTAB (N-cetyl-N,N, N-trimethyl ammonium bromide) was purchased from LOBA Chemie, India. Ethanol was supplied by Jiangsu Huaxi International Trade Co. Ltd, China. Deionized

water was obtained from Milli-Q water purification system (Millipores.A.S.67 120 Molsheim, France). All other reagents and chemicals used were of analytical grade.

### Methods of preparation of starch-coated $TiO_2$ nanocomposite

Coating of starch over $TiO_2$ particles was carried out in two steps following the method reported by Deka & Maji (2011). Initially $TiO_2$ was modified with CTAB and then was coated with starch.

### Preparation of CTAB-modified $TiO_2$ nanoparticles

One gram of $TiO_2$ was taken in a round-bottomed flask containing 1:1 ethanol–water mixture. The flask was fitted with a spiral condenser and kept at 80 °C for 12 h under magnetic stirring. In a similar set up, 1.2 g of CTAB was refluxed with 1:1 ethanol–water mixture at 80 °C for 3 h. This mixture was poured into the $TiO_2$ solution mixture and was stirred again for another 6 h at 80 °C. It was then filtered and washed with lukewarm deionized water several times and oven-dried at 45 °C. Finally, the material was ground and stored in a desiccator to avoid moisture absorption.

### Preparation of starch-coated CMT nanocomposite

One gram of CMT was dispersed in a 250 mL beaker under continuous magnetic stirring for 1 h and then sonicated for 30 min to completely disperse the CMT nanoparticles in the solvent.

In the meantime, a solution of starch was prepared by dissolving 0.5 g starch in 50 mL of hot water (80 °C). The CMT solution was then mixed with the starch solution and stirred for 1 h. Starch molecules typically have many –OH groups on them, which are polar. These –OH groups interact with the polar ends of CTAB and thus form a coating around them. The mixture was then poured slowly into acetone under stirring to precipitate the SPC particles.

The temperature of the beaker was brought down below room temperature, then glutaraldehyde solution (5% w/w) was added to the mixture containing SPC particles under magnetic stirring. The temperature was again raised gradually to 50 °C and the reaction was continued for another 2 h under continuous stirring condition. The temperature was then decreased to room temperature. The nanoparticles thus formed were filtered, washed with deionized water, dried and kept ready for subsequent applications.

### FT-IR analysis

Fourier transform infrared spectrophotometry (FT-IR) (NICOLET Impact I-410) was used to study the probable interaction between different component materials of the prepared nanoparticles as well as As(V) binding to the adsorbent. The study was carried out in the range 500–4,000 $cm^{-1}$.

### Thermogravimetry

Thermogravimetric analysis (TGA) was carried out for starch, UTi, CMT and SPC at a heating rate of 20 °C/min up to 500 °C under $N_2$ atmosphere using a thermogravimetric analyser (Metler TA 4000). The polymer content incorporated could be calculated using the following equation (Unsoy *et al.* 2012):

$$\text{Starch content } (\%) = W_s(\%) - W_n(\%) \quad (1)$$

where $W_s$ is the weight loss (%) from 100 °C to 500 °C for SPC and $W_n$ is the weight loss (%) for bare CMT nanoparticles.

### X-ray diffractometry

The distribution of the clay minerals within the polymer matrix in the nanoparticle was characterized by powder X-ray diffractometry (XRD) using a Miniflex instrument (Rigaku, UK). The measurement conditions were: anode material = Cu; K-alpha, $\lambda = 1.54$ Å and scanning rate 2°/min with an angle ranging from 2° to 80°.

### Scanning electron microscopy-electron dispersive X-ray analysis

A scanning electron microscope (SEM) (JEOL 6390LV) was used to study the presence of elements as well as morphology of the samples before and after As(V) treatment.

## pH measurement

The pH of the arsenic solutions was adjusted using NaOH (0.1 M) and/or HCl (0.1 M) solutions as required and measured by Cyberscan pH 510 (Eutech) instrument.

## Atomic absorption spectroscopic analysis

The As(V) concentration was measured by using an Analyst 200 Atomic Absorption Spectrophotometer (Perkin Elmer). All the measurements were based on integrated absorbance and performed at 193.7 nm by using a quartz tube analyser (Perkin Elmer) at an atomization temperature of 2,000 K.

## Batch adsorption experiments

A stock solution of 1,000 mg/L As(V) was prepared by dissolving the requisite amount of sodium arsenate ($Na_3AsO_4$) in 1,000 mL deionized water. The stock solution was diluted in steps to obtain standard solutions containing 0.1–0.7 mg/L of arsenic solution. The material dose and time for removal of As(V) was optimized by using the solution containing 400 μg As(V)/L. Batch adsorption studies were carried out with 2 g of adsorbent per litre of solution (as determined previously) of desired concentration at neutral pH in 100 mL conical flasks, which were agitated at 160 rpm for predetermined time intervals at room temperature on a mechanical shaker. After agitation, the suspension was centrifuged and filtered, and the arsenic concentration left in the aliquot was determined by atomic absorption spectrophotometry. A comparative study on the efficacy of UTi, CMT and SPC for As(V) removal was done.

The kinetic study for the adsorption of As(V) was conducted at neutral pH. In order to investigate the sorption mechanism for the removal process, pseudo first and second order kinetic models were used in different experimental conditions. The adsorption of As(V) was carried out for 90 min with initial As(V) concentration 0.1–0.7 mg/L for a material dose of 2 g/L. The kinetic parameters for sorption of As(V) for both CMT and SPC were calculated by using Lagergren's equations (Bhatt *et al.* 2012).

A simple pseudo first order kinetic model is represented as:

$$\log_{10}(q_e - q_t) = \log_{10} q_e - \frac{k_{ad}}{2.303} t \tag{2}$$

where, $q_t$ is the amount of As(V) adsorbed in mg/g at time t, $q_e$ is the amount of As(V) adsorbed (mg/g) at equilibrium and $K_{ad}$ is the rate constant of adsorption ($min^{-1}$).

The simplest and the most popular linear form pseudo second order kinetic models is represented by the following equation:

$$\frac{t}{q_t} = \frac{1}{h} + \frac{t}{q_e} \tag{3}$$

where $q_t = q_e{}^2 kt/(1 + q_t kt)$, the amount (mg/g) of As(V) adsorbed on the surface of material at any time $t$, $k$ being second order rate constant (g/mg min), $q_e$ is the amount adsorbed at equilibrium, and $h = kq_e^2$ (mg/g min) is the initial sorption rate.

Freundlich, Langmuir and Temkin isotherm models were applied for the study of equilibrium adsorption of As(V) on CMT and SPC.

The Langmuir isotherm is represented by the following equation (Ho 2006):

$$\frac{1}{q_e} = \frac{1}{q_m b}\frac{1}{C_e} + \frac{1}{q_m} \tag{4}$$

where, $q_e$ is the equilibrium quantity adsorbed (mg/g), $C_e$ is the equilibrium concentration (mg/L), $q_m$ is the maximum adsorption capacity (mg/g) and $b$ is the Langmuir constant.

The separation factor, $R_L$ an important parameter indicating the favourability of the adsorption based on the Langmuir equation is calculated using Equation (5).

$$R_L = \frac{1}{(1 + bC_0)} \tag{5}$$

where $b$ and $C_0$ have their common meaning. The value of $R_L$ indicates the type of adsorption either to be unfavourable ($R_L > 1$), linear ($R_L = 1$), favorable ($0 < R_L < 1$) or irreversible ($R_L = 0$).

The linear form of Freundlich adsorption equation is represented by the equation (Ho 2006):

$$\ln q_e = \ln K_f + \frac{1}{n} \ln C_e \quad (6)$$

where $q_e$ is the adsorbed amount (mg/g), $C_e$ is the equilibrium arsenic concentration (mg/L), $K_f$ (mg/g) is the Freundlich constant related to adsorption capacity and n is a constant related to energy of intensity of adsorption.

The Temkin model takes adsorbent–adsorbates interactions into account. By ignoring the extremely low and large value of concentrations, the model assumes that heat of adsorption (function of temperature) of all molecules in the layer would decrease linearly rather than logarithmically with coverage (Dada *et al.* 2012). The Temkin isotherm model is represented by the equation:

$$q_e = \frac{RT}{b} \ln A_T + \left(\frac{RT}{b}\right) \ln C_e \quad (7)$$

where $A_T$ = Temkin isotherm equilibrium binding constant (L/g), b = Temkin isotherm constant, R = universal gas constant (8.314 J/mol/K) and $T$ = temperature at 298 K; $q_e$ and $C_e$ have their common meaning.

## REUSABILITY STUDY

The reusability test was performed for CMT and SPC four times. An As(V) solution with an initial concentration of 400 μg/L was treated for 90 min with 2 g/L of CMT and SPC, respectively. It was then filtered and the concentration of As(V) in the filtrate was measured to determine the removal efficiency of the materials (CMT or SPC). The material left as residue was washed with dilute HCl acid for desorption of the As(V) ions adsorbed on its surface. It was then dried, weighed and used for further study to access the removal efficiency against the As(V) solution with same initial concentration. The process was repeated under the same conditions.

## RESULTS AND DISCUSSION

### Characterization

#### FT-IR analysis

FT-IR spectra of CTAB, UTi and CMT are shown in Figure 1(A). The FT-IR spectrum of UTi nanoparticles is shown in Figure 1(A(a)). The strong absorbance near 500 $cm^{-1}$ is attributable to the Ti–O–Ti stretching of $TiO_2$. The absorbance at 3,436–3,490 (–OH stretching) and 1,636 $cm^{-1}$ (–OH bending) are attributable to the surface hydroxyl groups of $TiO_2$ (Xu *et al.* 2010).

In the spectrum of CTAB, shown in Figure 1(A(b)), the absorption bands at 2,916 and 2,848 $cm^{-1}$, respectively, are attributable to asymmetric and symmetric modes of $-CH_2$ stretching in the methylene chains (Kungt & Hayes 1993). Band near 1,474 $cm^{-1}$ may be due to symmetric stretching of $CH_3^+$-N bond (Thakur 2015).

Bands near 2,916 $cm^{-1}$, 2,850 $cm^{-1}$ and 1,463 $cm^{-1}$ (corresponding to CTAB) along with bands at 1,636 $cm^{-1}$ and near 530 $cm^{-1}$ (corresponding to $TiO_2$) in the CMT spectrum indicate the probable interactions between the individual components.

Figure 1(B) shows the FT-IR spectra of starch, SPC and arsenic-treated SPC (ATC). The spectrum for starch (Figure 1(B(a))) shows a broad band near 3,440 $cm^{-1}$ for –OH stretching, 2,914 $cm^{-1}$ for –CH stretching and 1,656 $cm^{-1}$ for –OH bending. The two peaks in the region 1,183–966 $cm^{-1}$ are attributable to C–O bond stretching of C–O–H group (Kousalya *et al.* 2010). Incorporation of CMT into starch can be well predicted from the curve (b). Increase in intensity of bands corresponding to –OH stretching and –OH bending as well as appearance of a new band near 1,410 $cm^{-1}$ ($CH_3$–$N^+$ of CMT) is an indication for interaction between the two components.

In the FT-IR spectrum of ATC (Figure 1(B(c))), it was observed that the intensity of bands assigned to the hydroxyl groups and C–N stretching in SPC decreased prominently. This might be due to the participation of those groups in arsenic binding. The band appearing near 632 $cm^{-1}$ is attributable to the adsorbed arsenate ions on to the material (Sham *et al.* 1998).

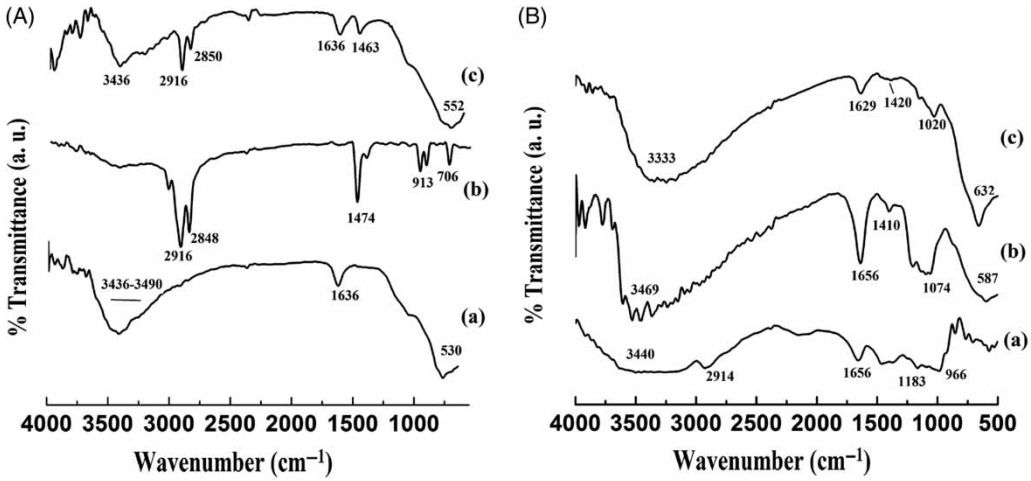


**Figure 1** | FT-IR spectra. (A) (a) UTi, (b) CTAB, (c) CMT. (B) (a) starch, (b) SPC, (c) ATC.

## SEM analysis

Figure 2(a)–2(d) show the SEM micrographs of UTi (a), CMT (b), SPC (c) and ATC (d). Sorption and desorption of arsenic for both SPC and CMT were done for four times using the same nanoparticles and then micrographs were taken. Figure 2(e) and 2(f) are micrographs of the used SPC and CMT.

CMT nanoparticles (Figure 2(b)) became less agglomerated than those of unmodified $TiO_2$ (Figure 2(a)) due to the presence of long hydrocarbon chains of CTAB which prevented them from agglomerating. Jiang *et al.* (2013) studied the morphology of CTAB-modified Ni nanoparticles and observed that modification with CTAB resulted in irregular sphere-like structures which were less aggregated than Ni-only nanoparticles. ATC (Figure 2(d)) composite appeared slightly rough compared to SPC (Figure 2(c)) composites. This might be due to sorbed arsenic on the composite structure. The surface of arsenic desorbed (i.e. reused) composite (Figure 2(e)) was rougher than SPC (Figure 2(c)). This might be attributed to the disintegration of the surface of the composite caused by the repeated

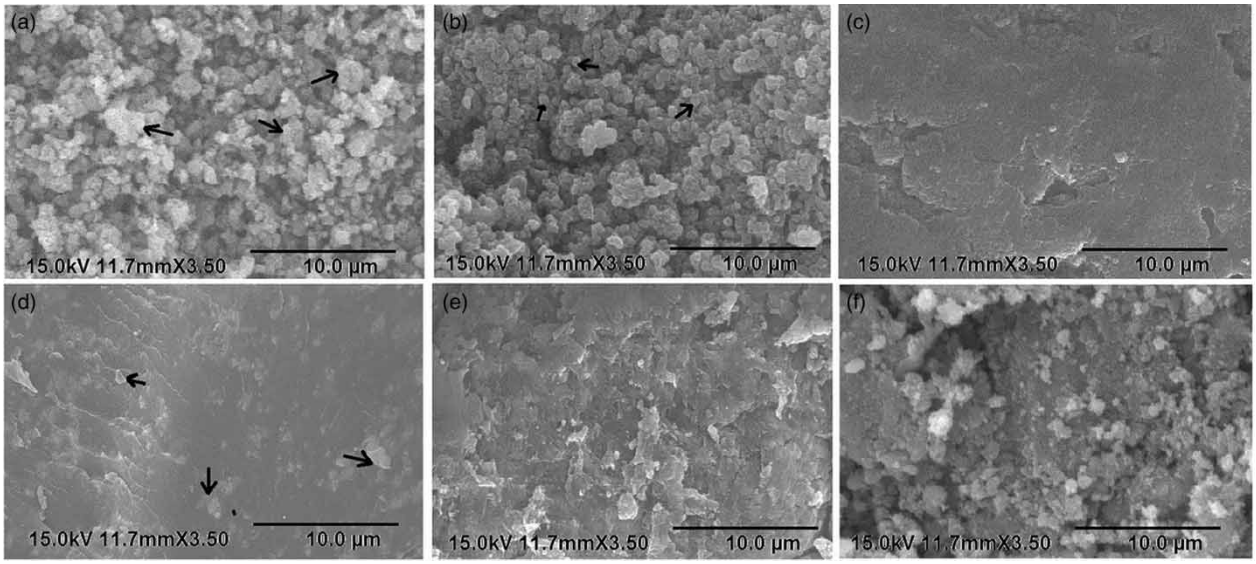


**Figure 2** | SEM images. (a) UTi, (b) CMT, (c) SPC, (d) ATC, (e) SPC/4 (used 4 times), (f) CMT/4 (used 4 times).

washing with acid during sorption-desorption treatment. Similarly the shape of CMT nanoparticles (Figure 2(f)) became irregular and rough due to the acid treatment.

## EDX study

Figure 3(a)–3(e) show the electron dispersive X-ray analysis (EDX) spectra of UTi, CTAB, CMT, SPC, arsenic treated CMT (AMT) and ATC, respectively. EDX spectra of UTi (Figure 3(a)) and CTAB (Figure 3(b)) show the presence of their corresponding elements in their structure. The spectrum shown in Figure 3(c) indicates the incorporation of bromine, carbon and nitrogen to the CMT particles. This confirms the successful modification of $TiO_2$ nanoparticles by CTAB.

The relative content of carbon and oxygen was greater in SPC (Figure 3(d)) than CMT (Figure 3(c)) suggesting the participation of starch polymer into the system. Presence of arsenic in the spectra of both arsenic adsorbed CMT and SPC confirmed the successful sorption of As(V) onto the systems. This further supports the findings of FT-IR data as discussed earlier (Figure 1(d)).

## TGA study

The thermograms for starch, UMT, CMT and SPC are shown in Figure 4(A). All four samples exhibited their own distinctive TGA curves. The initial weight loss observed in starch (Figure 4(A(a))) and SPC (Figure 4(A(d))) at around 100 °C was due to the evaporation of the small amount of moisture present in the samples.

The TGA curve for CMT (Figure 4(A(c))) shows some weight loss in the temperature range ~220–320 °C; UTi (Figure 4(A(b))) shows hardly any weight loss in that region. The weight loss in CMT is due to the incorporated CTAB on the surface of $TiO_2$ nanoparticles. Coating of CMT with starch in SPC showed much more weight loss as compared to CMT. But at the same time the weight loss was less than the pristine polymer. This indicated that interaction had taken place between CMT and starch, and starch had successfully coated the surface of CMT.

No separate degradation patterns were observed for the TGA curve of SPC indicating that the mixing of starch and CMT nanoparticles did not form a blend. Rather, starch properly interacted with CMT nanoparticles.

## XRD study

The XRD spectra of UTi, CMT and SPC are shown in Figure 4(B). The XRD patterns of UTi (Figure 4(B(b))) exhibit strong diffraction peaks at approximately $2\theta = 25^\circ$ (101), 37 ° (111), 47 ° (210), 53 ° (211) and 55 ° (220). The peaks occur due to the crystalline portion of the $TiO_2$. Similar findings were reported by Juang & Shiau (2000) and Wang *et al.* (2008). The diffraction peak at 21° is for crystallinity of starch.

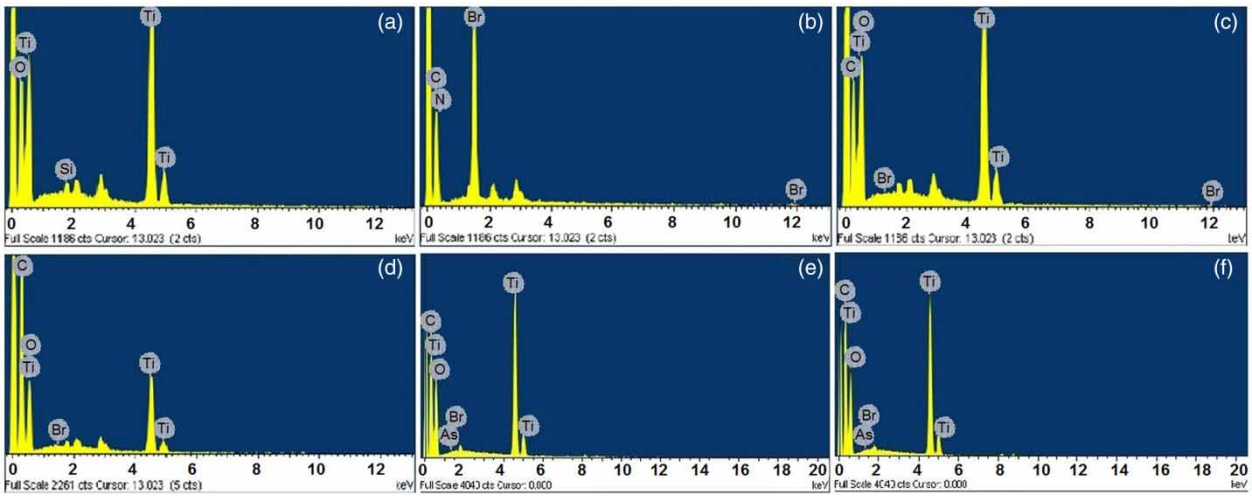


**Figure 3** | EDX spectra. (a) UTi, (b) CTAB, (c) CMT, (d) SPC, (e) AMT, (f) ATC.

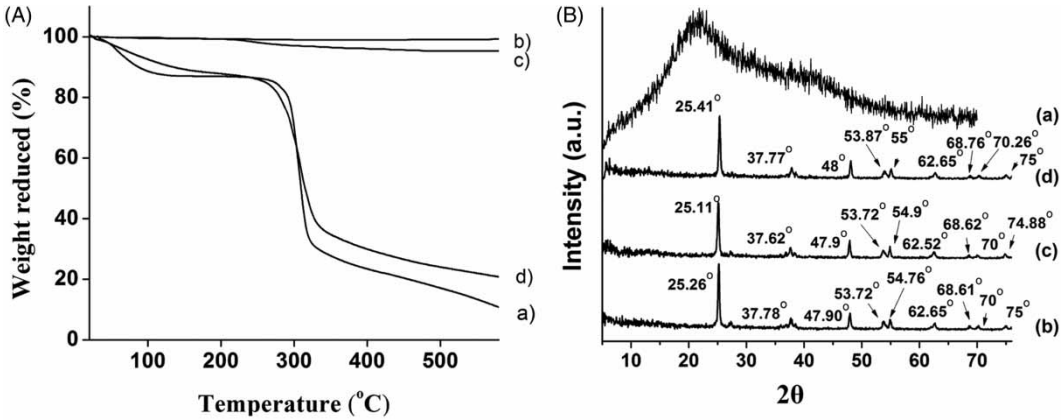


**Figure 4** | (A) TGA curves. (a) starch, (b) UTi, (c) CMT, (d) SPC. (B) XRD spectra. (a) starch, (b) UTi, (c) CMT, (d)SPC.

In the diffractogram of CMT (Figure 4(B(c))) and SPC (Figure 4(B(d))), no remarkable change in either peak positions/or peak intensity for $TiO_2$ crystals can be observed. This suggests that the starch coating process did not result in any phase change of $TiO_2$ particles.

## BATCH ADSORPTION EXPERIMENT FOR AS(V) REMOVAL

### Comparison of effectiveness of UTi, CMT and SPC towards As(V) removal

The effectiveness of UTi, starch, CMT and SPC materials for As(V) removal from contaminated water was tested. A targeted solution of 400 μg/L and material dose of 2 g/L were used. Starch alone did not produce any significant result. UTi, CMT and SPC showed good results as shown in Figure 5.

CMT particles exhibited better removal efficiency than UTi particles and brought down the arsenic concentration below 10 μg/L. CTAB prevented the aggregation of UTi particles and thus exposing more surfaces for interaction with arsenate ions in solution. However, part of the CMT entered into the aqueous phase during the experiment causing a significant loss of the material. This could be reduced by coating with crosslinked starch (SPC). Hence both CMT and SPC were used in the subsequent experiments.

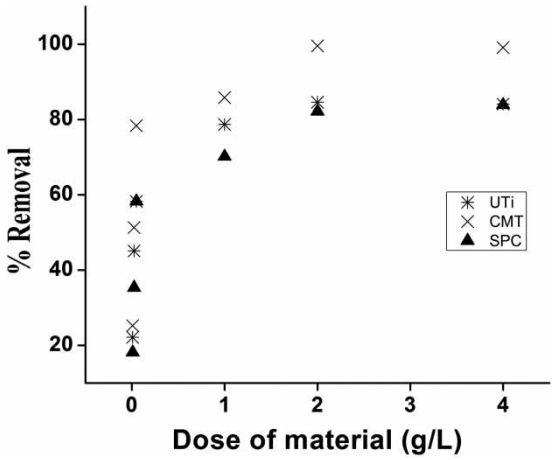


**Figure 5** | Efficacy of UTi, CMT and SPC for As(V) removal.

### Effect of material dosage on percentage removal of As(V)

The effect of material dose was studied by treating a laboratory-prepared arsenic(V) solution of known concentration with varying doses of CMT and SPC for about 5 h. Results are shown in Figure 6(a). Percentage removal of As(V) was plotted as a function of material dosage. On increasing material dosage of CMT and SPC, percentage removal of As(V) was observed to be increased.

It was found that for a solution of concentration 400 μg/L, a dose of 2 g/L of CMT was sufficient to bring down the As(V) concentration below 10 μg/L. No prominent change was observed with the increase of material dosage thereafter. Therefore, the material dose was fixed at 2 g/L for

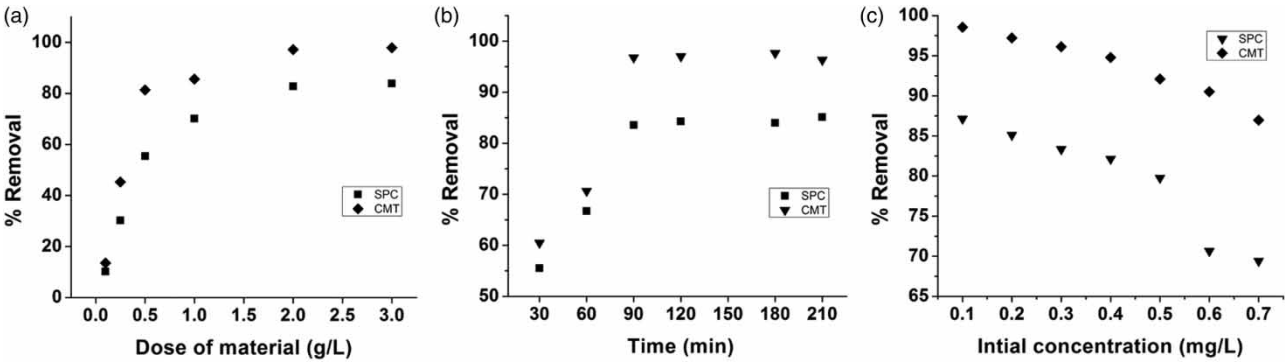


**Figure 6** | Effect of (a) material dose, (b) treatment time, (c) initial ion concentration on As(V) removal (%).

further study. Figure 6(a) shows that CMT has better efficiency compared to SPC for As(V) removal. However, reusability of CMT is a major problem as discussed later whereas starch coating is a good alternative.

### Influence of agitation time on arsenic removal

Figure 6(b) shows the effect of agitation time on percentage removal of the As(V) ion. With increase in treatment time, the percentage removal of As(V) reached maximum (99% for CMT and 83% for SPC) after 90 min treatment and after that remained almost constant throughout the time period studied. This might be due to the rapid achievement of equilibrium between the arsenic adsorbed on the surface of sorbent and arsenic present in solution. Therefore, the agitation time was kept fixed at 90 min for the subsequent batch experiments.

### Influence of initial As(V) concentration

The effect of initial arsenic(V) ion concentration was studied in the concentration range 0.1 to 0.7 mg/L. Material dose and agitation time were kept fixed as optimized before. Figure 6(c) shows the effect of As(V) concentration on percentage removal of the ion. With the increase in metal ion concentration, the amount of metal ion uptake per unit weight of adsorbent (mg/g) had also increased. It was observed that the percentage removal of As(V) decreased with the increase in initial metal ion concentration. This might be attributed to a delayed establishment of equilibrium between the adsorbent sites and the As(V) ions. The saturation of sorbent sites with the increase in initial ion concentration might also be the reason for diminished removal rate.

## ADSORPTION KINETICS

Figure 7(A) and 7(B) show the variation of adsorbed amount (mg/g) of arsenate ions over time for different initial ion concentrations for SPC and CMT, respectively. Additional plots of log ($q_e - q_t$) vs $t$ (Equation (2)) for the SPC and CMT gives straight lines from which the different pseudo first order kinetic parameters were evaluated (Table 1).

Similarly the different pseudo second order kinetics parameters were determined from the linear plot of $t/q_t$ vs $t$. The correlation coefficients ($R^2$) were computed and all the values are shown in Table 2. The $q_e$ values were found to increase with the increase in the initial As(V) concentrations. The curve for pseudo second order kinetics exhibited higher correlation co-efficient compared to pseudo first order model.

## EQUILIBRIUM ADSORPTION STUDY

Figure 8(a) and 8(b) show the growth of adsorbed amount (mg/g) at equilibrium over the surface of SPC and CMT, respectively, against increase in equilibrium concentrations. To establish the influence of As(V) concentration on the adsorption process, the equilibrium data has been analysed by linear forms of the Freundlich, Langmuir and Temkin models using Equations (4)–(6), respectively, and is shown in Table 3.

**Table 1** | Pseudo first order kinetic parameters for As(V) sorption

| | | CMT | | | SPC | | |
|---|---|---|---|---|---|---|---|
| $C_o$ (mg/L)[a] | M (g)[b] | $K_{ad}$ ($min^{-1}$) | $q_e$ (mg/g) | $R^2$ | $K_{ad}$ ($min^{-1}$) | $q_e$ (mg/g) | $R^2$ |
| 0.1 | 2 | $1.86\times10^{-02}$ | 0.142 | 0.949 | $2.05\times10^{-02}$ | 0.108 | 0.606 |
| 0.2 | 2 | $9.17\times10^{-03}$ | 0.202 | 0.780 | $3.22\times10^{-02}$ | 0.127 | 0.882 |
| 0.3 | 2 | $2.12\times10^{-02}$ | 0.335 | 0.923 | $3.05\times10^{-02}$ | 0.298 | 0.932 |
| 0.4 | 2 | $1.78\times10^{-02}$ | 0.450 | 0.953 | $2.70\times10^{-02}$ | 0.324 | 0.935 |
| 0.5 | 2 | $1.19\times10^{-02}$ | 0.487 | 0.924 | $1.69\times10^{-02}$ | 0.455 | 0.851 |
| 0.6 | 2 | $8.04\times10^{-03}$ | 0.528 | 0.869 | $2.18\times10^{-02}$ | 0.483 | 0.909 |
| 0.7 | 2 | $4.93\times10^{-03}$ | 0.630 | 0.773 | $5.51\times10^{-02}$ | 0.541 | 0.768 |

[a]$C_o$: Initial concentration of As(V) solution.
[b]M: Mass of CMT and SPC (adsorbent).

**Table 2** | Values of different second order kinetic parameters at different initial As(V) concentrations

| | | CMT | | | | SPC | | | |
|---|---|---|---|---|---|---|---|---|---|
| $C_o$ (mg/L)[a] | Mass (g)[b] | $q_e$ (mg/g) | K (g/mg min) | h (mg/g min) | $R^2$ | $q_e$ (mg/g) | K (g/mg min) | H (mg/g min) | $R^2$ |
| 0.1 | 2 | 0.196 | 0.633 | 0.025 | 0.995 | 0.174 | 6.221 | 0.189 | 0.999 |
| 0.2 | 2 | 0.354 | 0.568 | 0.071 | 0.998 | 0.362 | 0.271 | 0.035 | 0.990 |
| 0.3 | 2 | 0.597 | 0.154 | 0.055 | 0.992 | 0.538 | 0.148 | 0.043 | 0.988 |
| 0.4 | 2 | 0.767 | 0.112 | 0.066 | 0.988 | 0.707 | 0.094 | 0.047 | 0.980 |
| 0.5 | 2 | 0.868 | 0.148 | 0.112 | 0.995 | 0.809 | 0.085 | 0.056 | 0.971 |
| 0.6 | 2 | 0.962 | 0.197 | 0.182 | 0.997 | 0.889 | 0.076 | 0.059 | 0.968 |
| 0.7 | 2 | 1.010 | 0.297 | 0.304 | 0.998 | 1.091 | 0.052 | 0.062 | 0.945 |

[a]$C_o$: Initial concentration of As(V) solution.
[b]Mass of CMT and SPC (adsorbent).

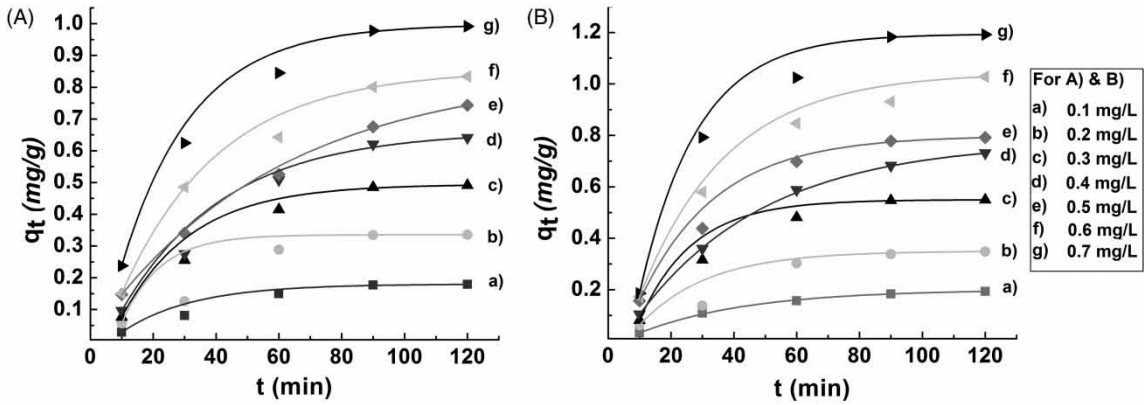


**Figure 7** | Time evalution of $q_t$ for different initial As(V) concentrations for (A) SPC and (B) CMT.

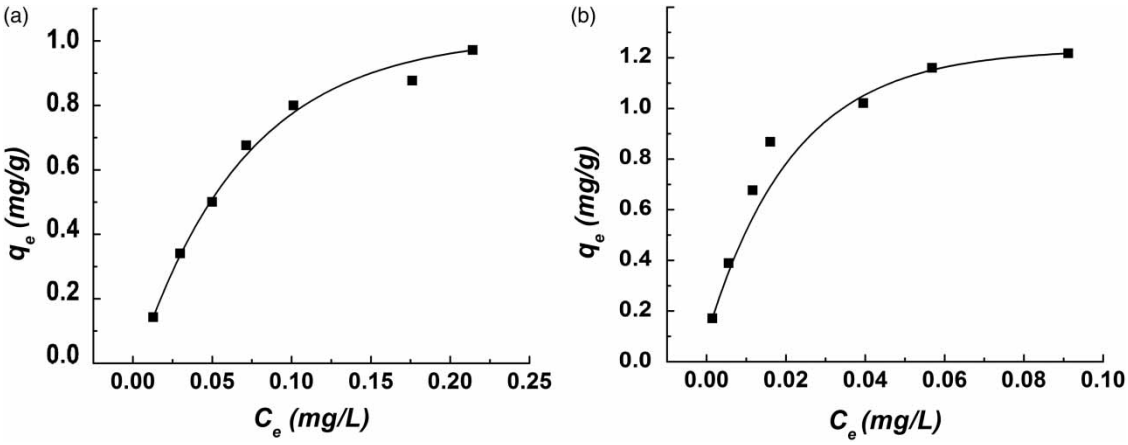


**Figure 8** | Variation of $q_e$ with $C_e$ for (a) SPC and (b) CMT.

The Langmuir parameters viz. $q_m$, b and $R^2$ values were found to be 1.024 mg/g, $1.31 \times 10^2$ and 0.989, respectively, for SPC and 1.423 mg/g, 10.82 and 0.998, respectively, for CMT.

In Table 3, it can be seen that the sorption was favourable for both materials as $R_L$ values (0.0187 for SPC and 0.187 for CMT) occurred between 0 and 1 for each case. Also $q_e$ vs $C_e$ showed a linear relationship.

Freundlich parameters $R^2$ and n values, as shown in Table 3, also indicated good fitting of sorption data with the model. The Temkin parameters were also derived and the correlation coefficient ($R^2 \sim 0.987$ and 0.984) values showed that Temkin model could well explain the sorption pattern.

**Table 3** | Sorption parameters of different isotherm model

| Model | SPC | | CMT | |
|---|---|---|---|---|
| Langmuir | $q_m$ (mg/g) | 1.024 | $q_m$ (mg/g) | 1.423 |
| | b (L/mg) | 131 | B (L/mg) | 10.82 |
| | $R^2$ | 0.989 | $R^2$ | 0.998 |
| | $R_L$ | 0.019 | $R_L$ | 0.187 |
| Freundlich | $K_f$ (mg/g) | 2.854 | $K_f$ (mg/g) | 2.751 |
| | n | 2.557 | n | 1.666 |
| | $R^2$ | 0.931 | $R^2$ | 0.944 |
| Temkin | $A_T$ (L/g) | $1.28 \times 10^3$ | $A_T$ (L/g) | $1.28 \times 10^2$ |
| | B (J g/mg$^2$) | $1.13 \times 10^4$ | B (J g/mg$^2$) | $8.62 \times 10^3$ |
| | $R^2$ | 0.987 | $R^2$ | 0.974 |

It was observed that the $R^2$ values for all the models showed good correlations of the data. Thus the sorption could be reasonably explained by all the models under consideration. The preferential order for sorption, among these models is as follows: Langmuir > Temkin > Freundlich.

A comparison of the maximum adsorption capacity ($q_o$) calculated from the Langmuir model with some other established materials is shown in Table 4. Ferruginous manganese ore has a high adsorption capacity as shown in Table 4, but arsenic does not get desorbed easily even on varying the pH (Chakravarty *et al.* 2002). The material under present investigation showed comparable results.

## RESUSABILITY TEST

Reusability experiments were carried out four times for both CMT and SPC. Each time the samples were treated with

**Table 4** | Comparison of adsorption capacity with other established material

| Material | Arsenic species | $q_o$ (mg/g) |
|---|---|---|
| $Fe_3O_4$-NPs (Akin *et al.* 2012) | As(V) | 0.400 |
| Chitosan-coated bentonite (Arida *et al.* 2015) | As(V) | 0.011 |
| Ferruginous manganese ore (Chakravarty *et al.* 2002) | As(V)<br>As(III) | 15.38<br>0.537 |
| SPC | As(V) | 1.024 |
| CMT | As(V) | 1.423 |

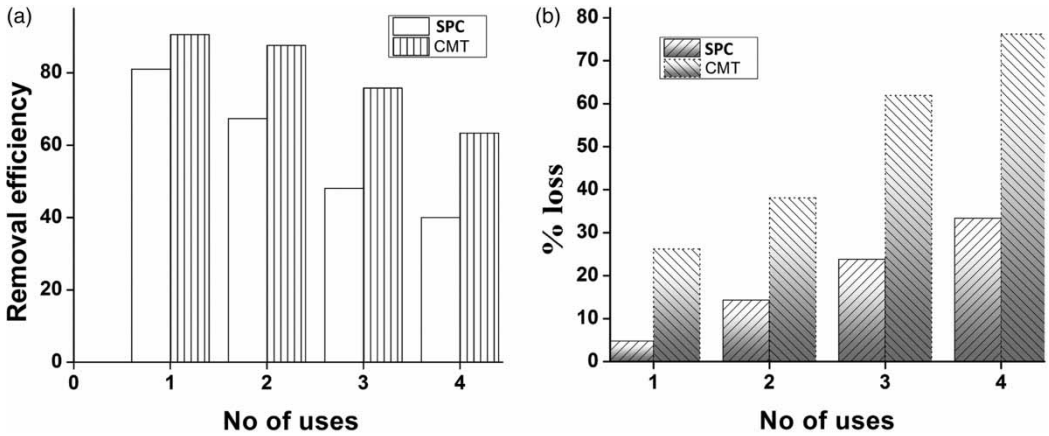


**Figure 9** | Comparison of (a) reusability, (b) weight remaining of CMT and SPC after reuse.

0.1 M HCl solution for desorption of the adsorbed As(V). The results are shown in Figure 9(a). As shown in the figure, CMT showed better As(V) removal efficiency than that of SPC under identical conditions.

The weight loss after each time of reuse was also calculated for both CMT and SPC. It was found that the weight loss (%) of material was low (Figure 9(b)) for SPC compared to CMT. This implied the successful stabilization of CMT particles inside the starch matrix resulting in a decreased leaching rate. Use of crosslinking agent also might have some contribution for observing lower weight loss in the case of SPC.

## Effect of competitive ions on removal of arsenate

The effect of competitive ions, i.e., phosphate and sulfate, on arsenate removal by CMT in synthetic water was investigated. Figure 10 shows the variation of the sorption rate of arsenate ions with the elevated concentration of phosphate and sulfate ions. The experiments were carried out with prepared solutions containing arsenate/phosphate and arsenate/sulfate ions at neutral pH. The change in removal rate was monitored with the elevated concentration of phosphate and sulfate ions in two separate experiments.

With the increase in their respective concentrations, both phosphate and sulfate ions were found to notably reduce the removal rate of arsenate. This might be due to the similarity in chemistry of As(V) with phosphate and sulfate in aqueous solution at neutral pH. The effect of

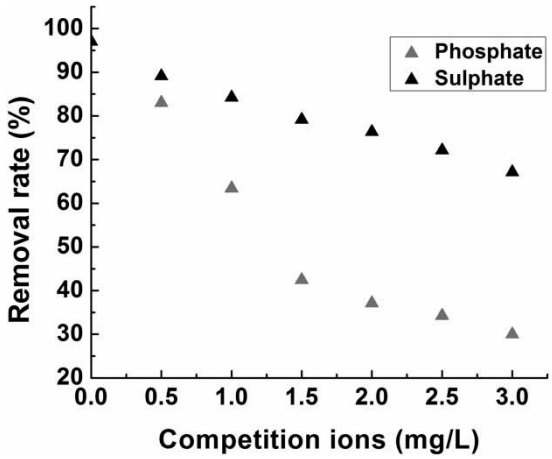


**Figure 10** | Effect of competition ions on removal As(V) by CMT.

phosphate is more pronounced (Figure 10) compared to that of sulfate. The resemblance of ionization constants and ionic structure of phosphate with arsenate is responsible for this anomaly (Guan *et al.* 2012).

## CONCLUSION

FT-IR analysis indicated successful modification of $TiO_2$ particles with CTAB surfactant. Good interaction of the modified form with starch polymer was also observed. These findings were further supported by TGA, SEM and EDX analysis. XRD data showed that the phase of $TiO_2$ remained unaltered during the modification or coating process. Successful sorption of As(V) was confirmed by FT-IR,

SEM and EDX analysis. Both CMT and SPC were capable of reducing the As(V) concentration from 400 μg/L to less than 10 μg/L.

The equilibrium data were fitted to Langmuir, Freundlich and Temkin adsorption isotherm models. The Langmuir isotherm model was found to be better fitted than the other two models as judged by their equilibrium data. The pseudo second order kinetic model showed better correlation than pseudo first order model for sorption of As(V) on CMT. Competitive ions like phosphate and sulfate reduce the arsenate removal rate by CMT.

Sorption of As(V) occurred in all the materials, i.e., UTi, CMT and SPC. SPC showed the best result when efficiency, reusability and integrity all are taken under consideration.

## ACKNOWLEDGEMENTS

The authors thank DRL, Tezpur for providing instrumental facilities.

## REFERENCES

Akin, I., Arslan, G., Tor, A., Ersoz, M. & Cengeloglu, Y. 2012 Arsenic(V) removal from underground water by magnetic nanoparticles synthesized from waste red mud. *J. Hazard. Mater.* **235–236**, 62–68.

An, B., Liang, Q. & Zhao, D. 2011 Removal of arsenic(V) from spent ion exchange brine using a new class of starch-bridged magnetite nanoparticles. *Water Res.* **45**, 1961–1972.

Arida, C. V. J., Luna, M. D. G. D., Futalan, C. M. & Wan, M.-W. 2015 Optimization of As(V) removal using chitosan-coated bentonite from groundwater using Box–Behnken design: effects of adsorbent mass, flow rate, and initial concentration. *Desalin. Water Treat.* **57**, 18739–18747.

Bang, S., Patel, M., Lippincott, L. & Meng, X. 2005 Removal of arsenic from groundwater by granular titanium dioxide adsorbent. *Chemosphere* **60**, 389–397.

Barakat, M. A. 2005 Adsorption behavior of copper and cyanide ions at $TiO_2$–solution interface. *J. Colloid Interface Sci.* **291**, 345–352.

Bhatt, A. S., Sakaria, P. L., Vasudevan, M., Pawar, R. R., Sudheesh, N., Bajaj, H. C. & Mody, H. M. 2012 Adsorption of an anionic dye from aqueous medium by organoclays: equilibrium modeling, kinetic and thermodynamic exploration. *RSC Adv.* **2**, 8663–8671.

Chakravarty, S., Dureja, V., Bhattacharyya, G., Maity, S. & Bhattacharjee, S. 2002 Removal of arsenic from groundwater using low cost ferruginous manganese ore. *Water Res.* **36**, 625–632.

Dada, A. O., Olalekan, A. P., Olatunya, A. M. & Dada, O. 2012 Langmuir, Freundlich, Temkin and Dubinin–Radushkevich isotherms studies of equilibrium sorption of $Zn^{2+}$ Unto phosphoric acid modified rice husk. *J. Appl. Chem.* **3**, 38–45.

Daimei, C., Dong, Y., Qun, W. & Zhongyi, J. 2006 Effects of boron doping on photocatalytic activity and microstructure of titanium dioxide nanoparticles. *Ind. Eng. Chem. Res.* **45**, 4110–4116.

Debnath, S. & Ghosh, C. U. 2009 Nanostructured hydrous titanium(IV) oxide: synthesis, characterization and Ni(II) adsorption behavior. *Chem. Eng. J.* **152**, 480–491.

Deka, B. K. & Maji, T. K. 2011 Effect of $TiO_2$ and nanoclay on the properties of wood polymer nanocomposite. *Composites Part A* **42**, 2117–2125.

Dutta, P. K., Ray, A. K., Sharma, V. K. & Millero, F. J. 2004 Adsorption of arsenate and arsenite on titanium dioxide suspensions. *J. Colloid Interf. Sci.* **278**, 270–275.

Gautham, J., Souhail, R. A.-A., Vijayakumar, S., Hyeok, C., Kirk, G. S. & Dionysios, D. D. 2010 Arsenic sorption on $TiO_2$ nanoparticles: size and crystallinity effects. *Water Res.* **44**, 965–973.

Ghosh, C. U., Dasgupta, M. & Debnath, S. 2003 Studies on management of chromium(vi)-contaminated industrial waste effluent using hydrous titanium oxide. *Water, Air, Soil Pollut.* **143**, 245–256.

Guan, X., Du, J., Meng, X., Sun, Y., Sun, B. & Hu, Q. 2012 Application of titanium dioxide in arsenic removal from water: a review. *J. Hazard. Mater.* **215–216**, 1–16.

Gupta, S. M. & Tripathi, M. A. 2011 Review of $TiO_2$ nanoparticles. *Chin. Sci. Bull* **56**, 1639–1652.

Gupta, K. K., Singh, N. L., Pandey, A., Shukla, S. K., Upadayay, S. N., Mishra, V., Srivastava, P., Lalla, N. P. & Mishra, P. K. 2012 Effect of anatase/rutile $TiO_2$ phase composition on arsenic adsorption. *J. Dispersion Sci. Technol.* **34**, 1043–1052.

He, F. & Zhao, D. 2005 Preparation and characterization of a new class of starch-stabilized bimetallic nanoparticles for degradation of chlorinated hydrocarbons in water. *Environ. Sci. Technol.* **39**, 3314–3320.

Ho, Y.-S. 2006 Isotherms for the sorption of lead onto peat: comparison of linear and non-linear methods. *Pol. J. Environ. Stud.* **15**, 81–86.

Jiang, Z., Xie, J., Jiang, D., Wei, X. & Chen, M. 2013 Modifiers-assisted formation of nickel nanoparticles and their catalytic application top-nitrophenol reduction. *Cryst. Eng. Comm.* **15**, 560–569.

Juang, R. S. & Shiau, R. C. 2000 Metal removal from aqueous solutions using chitosan-enhanced membrane filtration. *J. Membr. Sci.* **165**, 159–167.

Kajitvichyanukul, P., Ananpattarachai, J. & Pongpom, S. 2005 Sol–gel preparation and properties study of $TiO_2$ thin film for photocatalytic reduction of chromium(VI) in photocatalysis process. *Sci. Technol. Adv. Mater.* **6**, 352–358.

Keliang, S., Xuefeng, W., Zhijun, G., Shengrong, W. & Wangsuo, W. 2009 Se(IV) sorption on $TiO_2$: sorption kinetics and surface

complexation modeling. *Colloid. Surf. A: Physicochem. Eng. Aspects.* **349**, 90–95.

Kousalya, G. N., Gandhi, M. R. & Meenakshi, S. 2010 Sorption of chromium(VI) using modified forms of chitosan beads. *Int. J. Biol. Macromol.* **47**, 308.

Kungt, K.-H. S. & Hayes, K. F. 1993 Fourier transform infrared spectroscopic study of the adsorption of cetyltrimethylammonium bromide and cetylpyridinium chloride on silica. *Langmuir* **9**, 263.

Marques, A. P., Reis, R. L. & Hunt, J. A. 2002 The biocompatibility of novel starch-based polymers and composites: in vitro studies. *Biomaterials* **23**, 1471–1478.

Miao, Y., Zhang, Z., Gong, Y., Zhang, Q. & Yan, G. 2014 Self-assembly of manganese doped zinc sulfide quantum dots/CTAB nanohybrids for detection of rutin. *Biosens. Bioelectron.* **52**, 271–276.

Nakajima, T., Xu, Y.-H., Mori, Y., Kishita, M., Takanashi, H., Maeda, S. & Ohki, A. 2005 Combined use of photocatalyst and adsorbent for the removal of inorganic arsenic(III) and organoarsenic compounds from aqueous media. *J. Hazard. Mater.* **120**, 75–80.

Saikia, J. P., Banerjee, S., Konwar, B. K. & Kumar, A. 2010 Biocompatible novel starch/polyaniline composites: characterization, anti-cytotoxicity and antioxidant activity. *Colloids Surf. B Biointerfaces* **81**, 158–164.

Sham, E. L., Miguel, A. G., Aranda, E., Farfan-Torres, M., Gottifredi, J. C., Martinez-Lara, M. & Bruque, S. 1998 Zirconium titanate from sol–gel synthesis: thermal decomposition and quantitative phase analysis. *J. Solid State Chem.* **139**, 225–232.

Thakur, V. K. 2015 *Lignocellulosic Polymer Composites.* Scrivener Publishing, Beverly, MA, USA

Unsoy, G., Yalcin, S., Khodadust, R., Mutlu, P. & Gunduz, U. 2012 Nanocon. 23–25.10.2012, Brno, Czech Republic.

Wang, H., Liu, P., Cheng, X., Shui, A. & Zeng, L. 2008 Effect of surfactants on synthesis of $TiO_2$ nano-particles by homogeneous precipitation method. *Powder Technol.* **188**, 52–54.

Xiaobo, C. & Samuel, S. M. 2007 Titanium dioxide nanomaterials: synthesis, properties, modifications, and applications. *Chem. Rev.* **107**, 2891–2959.

Xu, T., Cai, Y. & O'Shea, K. E. 2007 Adsorption and photocatalyzed oxidation of methylated arsenic species in $TiO_2$ suspensions. *Environ. Sci. Technol.* **41**, 5471–5477.

Xu, Z., Li, Q., Gao, S. & Shang, J. K. 2010 As(III) removal by hydrous titanium dioxide prepared from one-step hydrolysis of aqueous $TiCl_4$ solution. *Water Res.* **44**, 5713–5721.

Zhang, F.-S. & Itoh, H. 2006 Photocatalytic oxidation and removal of arsenite from water using slag-iron oxide-$TiO_2$ adsorbent. *Chemosphere* **65**, 125–131.

First received 17 May 2016; accepted in revised form 1 August 2016. Available online 3 November 2016